

Accepted Manuscript

Two new lanthanide-nitronyl nitroxide complexes: magnetic and fluorescence properties

Pei-Pei Sun, Shuai-Liang Yang, Chen-Xi Zhang, Qing-Lun Wang

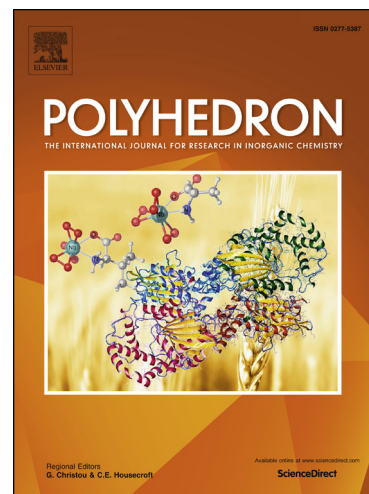
PII: S0277-5387(18)30587-4
DOI: <https://doi.org/10.1016/j.poly.2018.09.035>
Reference: POLY 13434

To appear in: *Polyhedron*

Received Date: 25 May 2018
Accepted Date: 15 September 2018

Please cite this article as: P-P. Sun, S-L. Yang, C-X. Zhang, Q-L. Wang, Two new lanthanide-nitronyl nitroxide complexes: magnetic and fluorescence properties, *Polyhedron* (2018), doi: <https://doi.org/10.1016/j.poly.2018.09.035>

This is a PDF file of an unedited manuscript that has been accepted for publication. As a service to our customers we are providing this early version of the manuscript. The manuscript will undergo copyediting, typesetting, and review of the resulting proof before it is published in its final form. Please note that during the production process errors may be discovered which could affect the content, and all legal disclaimers that apply to the journal pertain.



Two new lanthanide-nitronyl nitroxide complexes: magnetic and fluorescence properties

Pei-Pei Sun ^a, Shuai-Liang Yang ^b, Chen-Xi Zhang ^{ab} and Qing-Lun Wang ^{cd}

^aCollege of Chemical Engineering and Materials Science, Tianjin University of Science and Technology, Tianjin 300457, P. R. China

^bKey Laboratory of Advanced Energy Materials Chemistry (Ministry of Education), Nankai University, Tianjin 300071, P. R. China

^cCollege of Chemistry, Nankai University, Tianjin 300071, P. R. China

ABSTRACT

Two new lanthanide complexes of nitronyl nitroxide radical have been synthesized and characterized on the structure, magnetism and fluorescence: $[\text{Ln}(\text{hfac})_3(\text{NITPh}(\text{OCH}_3)_2)_2]$ ($\text{Ln}=\text{Tb}(\mathbf{1}), \text{Dy}(\mathbf{2})$), (NITPh-(OCH₃)₂=2-(3',4'-dimethoxy-phenyl)-4,4,5,5-tetramethyl-imidazoline-1-oxyl-3-oxide); hfac=hexafluoroacetylacetonate). Two complexes crystallize in monoclinic space group C2/c, which have similar mononuclear structures. The central metal ion is eight coordinated by six oxygen atoms from three hfac molecules and two oxygen atoms from two nitronyl nitroxide radicals. The varying temperature magnetic susceptibility indicates that there are weak antiferromagnetic interaction between metal ions and nitronyl nitroxide radicals in complexes **1** ($zJ' = -0.145 \text{ cm}^{-1}$) and **2** ($zJ' = -0.140 \text{ cm}^{-1}$). AC magnetic susceptibility studies exhibit no single-molecule magnet behavior in complexes **1** and **2**. In addition, the fluorescence properties of **1** show that it is an excellent fluorescent probe of recognizing Cr₂O₇²⁻ anion. Because of the linear relationship at low concentration and detection limit reached $1 \times 10^{-7} \text{ M}$, it can be used as a luminescence-based sensor for quantitative analysis.

Keywords: Nitronyl nitroxide; Lanthanides; Magnetic properties; Luminescence properties

1. Introduction

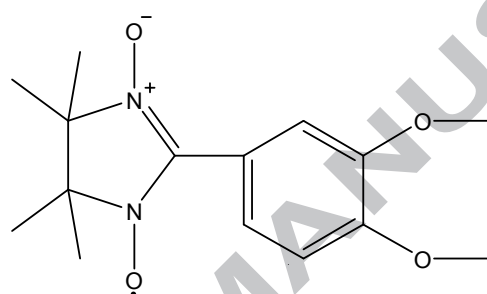
In recent years, the unique structure and properties of nitronyl nitroxide radical have attracted many researchers due to their advantages such as good chemical stability, versatility, easy to modify^[1-2]. The metal-radical method has been proved to be one of the most effective methods for synthesizing molecular-based magnetic materials^[3-4]. Based on the electronic arrangement rule, the 4f electron orbit of lanthanide ions is effectively shielded by the outer-shell electrons. Furthermore, lanthanide ions have large anisotropic magnetic moments, the energy barrier value increases obviously, therefore magnetic characteristics of lanthanide ions are difficult to be analyzed^[5]. To explore the magnetic properties of lanthanide-radical complexes, different types of lanthanide complexes with nitronyl nitroxide radicals were synthesized^[6]. Tb(III) and Dy(III) ions have large magnetic anisotropies and become an ideal choice for constructing SMMs and SCMs^[7-8], especially since the first 4f-2p SMM [Dy(hfac)₃NITpPy] was reported^[9]. Hence, we decided to use Tb and Dy ions combined with new nitronyl nitroxide radicals to obtain single-molecule magnets.

Lanthanide metal with light physical characteristics of photochemical stability, long fluorescence lifetime, emission wavelength and large Stokes shift, can avoid the

* Corresponding author. Email: zcx@tust.edu.cn

interference of stray light and fluorescence system itself, thus greatly increases the sensitivity of the sensor^[10]. Therefore, lanthanide metal complexes have been widely used for the sensation of biological anions, metal ions, and oxides^[11].

In order to detect the new lanthanide-radical magnetic coupling systems and to better understand the properties of 4f-2p magnetic interactions, two mononuclear lanthanide-radical complexes ($[\text{Ln}(\text{hfac})_3(\text{NITPh}-(\text{OCH}_3)_2)_2]$ ($\text{Ln}=\text{Tb}(\mathbf{1}), \text{Dy}(\mathbf{2})$) were synthesized successfully by using a new nitronyl nitroxide radical ($\text{NITPh}-(\text{OCH}_3)_2=2-(3',4'\text{-dimethoxy-phenyl})-4,4,5,5\text{-tetramethyl-imidazoline-1-oxyl-3-oxide}$) (Scheme 1). Their crystal structures and magnetic properties were described in this paper. Meanwhile, the luminescence characteristics of complex **1** show the characteristic emission peaks of Tb(III) ions and the ability to recognize $\text{Cr}_2\text{O}_7^{2-}$. Therefore, complex **1** can be used as a luminescence-based sensor for the quantitative and sensitive detection of $\text{Cr}_2\text{O}_7^{2-}$.



Scheme 1. Structure of the $\text{NITPh}-(\text{OCH}_3)_2$

2. Experimental

2.1. General

All of the reagents and solvents are of analytical grade without purification. $\text{Ln}(\text{hfac})_3 \cdot 2\text{H}_2\text{O}$ ($\text{Ln}=\text{Tb}(\mathbf{1}), \text{Dy}(\mathbf{2})$)^[12] and $\text{NITPh}-(\text{OCH}_3)_2$ ^[13] were synthesized according to known methods. C, H and N were analyzed on a Model 240 Perkin-Elmer elemental analyzer. Complexes **1** and **2** were measured using a WGH-30A double beam infrared spectrophotometer with KBr tablets in the $4000\text{-}400\text{cm}^{-1}$ range. The PXRD was recorded on the Shimadzu Labx XRD-6100 diffractometer using the Cu target tube and the graphite monochromator, and operated under the 40kV and 30.0mA. The intensity data were continuously scanned from 5° to 50° degrees in $2\theta/\theta$ mode, with the step length of 0.02° and the scan speed of 5° min^{-1} . MPMS-7 SQUID magnetometer recorded magnetic data. The diamagnetic corrections were carried out by the Pascal's constants for all the atoms^[14]. Luminescence characteristics were recorded on F-280FL spectrophotometer. UV-vis spectral data were recorded by TU-1901. The infrared absorption peak and UV-vis spectral data of complexes **1** and **2** are listed in Table S1-S2.

2.2. Synthesis of $\text{NITPh}-(\text{OCH}_3)_2$

2.2 g of 3,4-dimethoxybenzaldehyde was added to 3.1 g of 2,3-dimethyl butane-2,3-hydroxylamine^[13], and the reaction was stirred magnetically for 24 hours at room temperature. A precipitate formed, the mixture was suction filtered, washed several times with anhydrous ethanol, and dried in a vacuum oven at 40°C for 12 hours to crush the white product into a powder. Then, 2.1 g powder was added to 63 mL of dichloromethane, then 3.0 g of a saturated solution of sodium periodate was added, magnetically stirred at room temperature, the mixture turned from white to dark blue. The reaction was carried out

for one hour. After concentrating and purifying, the filtrate volatilize in at room temperature and dark blue crystals were obtained. The yield was 58%.

2.3. Synthesis of $[Ln(hfac)_3(NITPh-(OCH_3)_2)_2](Ln=Tb(\mathbf{1}), Dy(\mathbf{2}))$

21 mg (0.025 mmol) of $Tb(hfac)_3 \cdot 2H_2O$ was added in 15 mL of N-heptane. The mixture was magnetically stirred and refluxed at 110°C for 2 hours, cooled to 80°C, and then a solution of NITPh-(OCH₃)₂ dissolved in 3 mL of CH₂Cl₂ was added. After refluxing for 30 min, the mixture was cooled and filtered, the filtrate was placed in a beaker, tardily volatilize at about 4°C. Dark blue rhombohedral crystals suitable for X-ray diffraction analysis were obtained after several days. Anal.Calcd(1) for C₄₅H₄₅TbF₁₈N₄O₁₄ (Yield:41%): C, 39.50%, H, 3.29%, N, 4.10%; found: C, 39.37%, H, 3.48%, N, 4.18%. IR (KBr, cm⁻¹): 3494 (m), 2957(w), 3023(w), 1385(m), 1374(s), 1322(s), 1212(s).

The preparation of complex **2** is the same procedure as that of complex **1**, but using Dy(hfac)₃·2H₂O instead of Tb(hfac)₃·2H₂O. Anal.Calcd(2) for C₄₅H₄₅DyF₁₈N₄O₁₄ (Yield: 39 %): C, 39.41%, H, 3.28%, N, 4.09%; found: C, 38.97%, H, 3.31%, N, 4.23%. IR (KBr, cm⁻¹): 3502(m), 2931(w), 3101(w), 1330(m), 1362(s), 1294(s), 1217(s).

2.4. Crystal structure determination

The crystal structures data of complexes **1** and **2** were determined using a Bruker SMART type 1000 X-ray diffractometer, using Mo K α radiation ($\lambda = 0.7107 \text{ \AA}$) monochromatized by a graphite monochromator at 113K. The diffraction points were collected by ω - ψ scan method, the non-hydrogen atomic coordinates were solved by direct method, and the coordinates and anisotropic thermal parameters were corrected by the least square method. Hydrogen atoms were generated theoretically at the specific atoms and refined isotropically with fixed thermal factors^[15]. All computations and corrections were implemented using the SHELXTL (olex 2) package^[16]. The crystallographic data of the obtained complexes are shown in Table 1.

Table 1. Crystal structure data and processing parameters for complexes **1-2**.

| Complexes | 1 | 2 |
|--|--|--|
| Empirical formula | C ₄₅ H ₄₅ TbF ₁₈ N ₄ O ₁₄ | C ₄₅ H ₄₅ DyF ₁₈ N ₄ O ₁₄ |
| Formula weight | 1366.77 | 1370.35 |
| T/ K | 113(2) | 113(2) |
| Color | Dark blue | Dark blue |
| Crystal system | monoclinic | monoclinic |
| Space group | C2/c | C2/c |
| a(Å) | 20.911(10) | 20.9451(4) |
| b(Å) | 11.500(6) | 11.5010(3) |
| c(Å) | 22.945(12) | 23.0265(4) |
| α (°) | 90.00 | 90.00 |
| β (°) | 91.334(17) | 91.4300(18) |
| γ (°) | 90.00 | 90.00 |
| Z | 4 | 4 |
| Volume (Å ³) | 5516(5) | 5545.1(2) |
| Calculated density(mg/m ³) | 1.646 | 1.628 |
| Absorption coefficient (mm ⁻¹) | 1.407 | 1.411 |
| F(000) | 2728 | 2732 |

| | | |
|---|-------------------|-------------------|
| θ range for data collection ($^{\circ}$) | 3.233 to 27.588 | 3.208 to 27.421 |
| Reflections | 32875 / 15732 | 32678 / 11827 |
| collected/unique | [R(int) = 0.0107] | [R(int) = 0.0268] |
| Goodness-of-fit on F^2 | 1.067 | 1.053 |
| $RI[I > 2\sigma(I)]$ | 0.0287 | 0.0323 |
| $wR2[I > 2\sigma(I)]$ | 0.0967 | 0.1897 |
| RI (all data) | 0.0643 | 0.0559 |
| $wR2$ (all data) | 0.1429 | 0.2013 |

2.5. The process of fluorescence study

The luminescent characteristics of complex **1** were studied in aqueous solution at room temperature. For sensing of anions, 4 mg of the powder sample of complex **1** was dispersed in 8 ml of salt solution K_yX ($X = Cl^-, SO_4^{2-}, Br^-, NO_3^-, I^-$, and $Cr_2O_7^{2-}$, $y = 1$ or 2 , 1 mM) and sonicated to form a suspension for fluorescence studies at room temperature. (slit = 10 nm, PMT voltage = 950 V, scan rate = 1200 nm / min)

3. Results and discussion

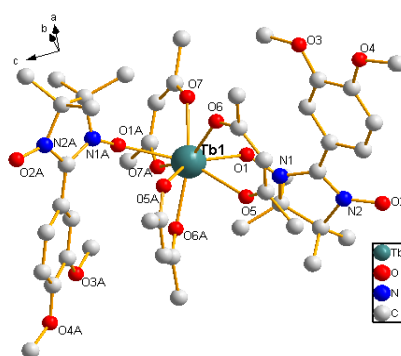
3.1. Description of the crystal structures

Single-crystal X-ray diffraction analysis showed that complexes **1** and **2** crystallize in monoclinic $C2/c$ space group. They have similar mononuclear tri-spin structures (Figs. 1 and S1). The coordination polyhedron of complexes **1** and **2** can be described as a twisted dodecahedron with triangular faces^[17]. The crystal structure of complex **1** is described as an example. The Tb(III) ion is eight coordinated by six oxygen comes from three hfac, with the Tb- O_{hfac} bond length is in the range of 2.332(1)-2.409(1) Å, which is similar to other Tb-nitroxide radicals complexes previously reported^[18-19]. Another two oxygen atoms come from two NITPh-(OCH_3)₂ with the Tb- O_{Rad} bond of 2.331(1) Å. The uncoordinated N-O bond length (1.271(2) Å) is shorter than the coordinated N-O bond length (1.307(2) Å). The bond angle of the O_{Rad} -Tb- O_{Rad} is 142.030(4) $^{\circ}$. The dihedral angle formed by five atoms on the O-N-C-N-O moieties of the nitronyl nitroxide radicals and benzene ring is 25.227(60) $^{\circ}$. The selected bond lengths and angles of complex **1** are shown in Table S3.

Fig. 1. The molecular structure of complex **1** (Hydrogen atoms and fluorine atoms are not shown)

For complex **2**, due to the substitution of the crystal parameters, bond lengths slightly different. The bond length of Dy- O_{hfac} is between 2.328(1)-2.328(1) Å to the data reported in the literature^[18-21]. The bond length of Dy- O_{Rad} is 2.325(1) Å. The uncoordinated N-O bond length (1.278(0) Å) is also shorter than the coordinated N-O bond length (1.305(0) Å). The major bond lengths and angles of complex **2** are shown in Table S4.

There are three types of hydrogen bonds in complex **1**, which are C3-H13B \cdots F6 (2.502(2) Å), C14-H14A \cdots O2 (2.598(2) Å), and C15-H15B \cdots O3 (2.514(2) Å) (Fig. S2). The C3-H13B \cdots F6 combines adjacent molecules into one-dimensional chains. The one-



of complex **1** (Hydrogen atoms and fluorine atoms are not shown)

the lanthanide contraction, central ions causes the angles and bond lengths the literature^[18-21]. The

dimensional chains are connected by C14-H14A \cdots O2 to form a two-dimensional planar structure and then through C15-H15B \cdots O3 further form a three-dimensional supramolecular network structure. There are two types of hydrogen bonds in complex **2**, which are C1-H1A \cdots F4 (2.52 (2) Å) and C12-H12C \cdots O4 (2.55 (2) Å). In Fig. S3, it can be seen that due to the hydrogen bonding, complex **2** formed a 3D supermolecular network structure. The lengths and angles of the intermolecular hydrogen bonds of complexes **1** and **2** are listed in Table S5.

3.2. Powder X-ray Diffraction

In order to determine whether the crystal structure really represents bulk material, the X-ray powder diffraction patterns of complexes **1** and **2** are shown in Fig. S4 and S5. The PXRD patterns are consistent with the results of a single crystal data simulation, reflecting the purity of the synthesized bulk material.

3.3. Magnetic property for complexes **1** and **2**

Temperature-dependent magnetic susceptibility tests for complexes **1** and **2** were done under the conditions of an applied magnetic field of 1000 Oe and a temperature range of 2-300 K. The temperature dependence of χ_M and $\chi_M T$ are shown in Figs. 2 and 3. The $\chi_M T$ value of complex **1** at room temperature is 12.64 cm³ K mol⁻¹, which is slightly higher than the theoretical value 12.56 cm³ K mol⁻¹ for uncoupled single Tb(III) ion (⁷F₆, S=3, L=3, g = 3/2, C=11.82 cm³ K mol⁻¹) plus two radicals (S = 1/2). With the temperature decreasing, the $\chi_M T$ value slightly increase from 300 - 80 K and then decreases sharply at low temperature, reaching the minimum value of 4.09 cm³ K mol⁻¹ at 2 K. This phenomenon may be due to the weak antiferromagnetism between Tb(III) ion and nitronyl nitroxide radicals and the depopulation of Ln(III) Stark energy level caused by crystal field disturbance. For complex **2**, at room temperature, the magnetic moment $\chi_M T$ value is about 14.99 cm³ K mol⁻¹, which is resemblance to the theoretical value 14.92 cm³ K mol⁻¹ for uncoupled single Dy(III) ion (⁶H_{15/2}, S=5/2, L=5, g = 4/3, C=14.17cm³ K mol⁻¹) plus two radicals (S = 1/2, 0.375 cm³ K mol⁻¹). Upon cooling, the $\chi_M T$ value decreases steadily and reached the minimum value of 6.01 cm³ K mol⁻¹ at 2 K.

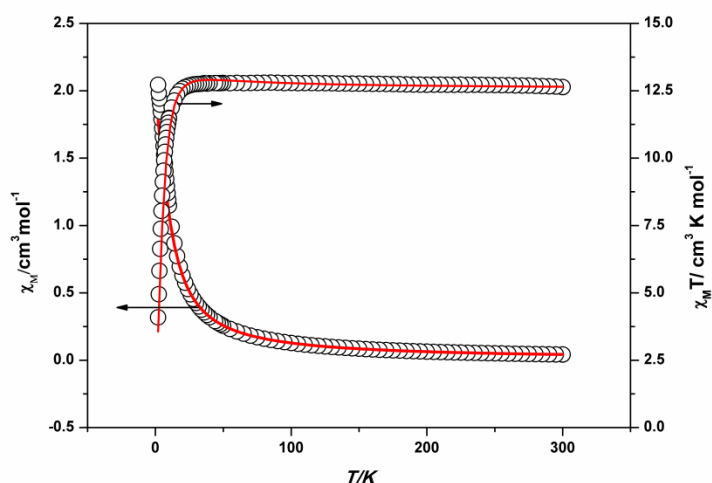


Fig. 2. Temperature dependence of χ_M (bottom) and $\chi_M T$ (top) of complex **1** at 1000 Oe.

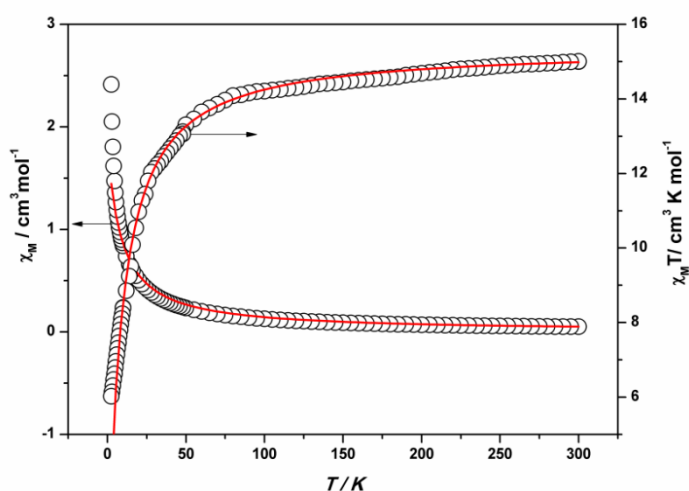


Fig. 3. Temperature dependence of χ_M (bottom) and $\chi_M T$ (top) of complex **2** at 1000 Oe.

Due to the large anisotropy of Ln(III) (Ln=Tb, Dy), it is difficult to apply a strict magnetic interaction theory to this tri-spin system. Therefore, in order to roughly estimate the magnetic interactions in the tri-spin molecule, we used the approximate model for complexes **1** and **2** with equation (1)-(3) in SI^[22-23]. The χ_{Tb} and χ_{Dy} can be described by the formula equation (4) and (5) in SI, respectively.

The best fitting parameters are $g = 1.50$, $\Delta = -0.56 \text{ cm}^{-1}$, $zJ' = -0.145 \text{ cm}^{-1}$ for complex **1** and $g = 1.36$, $\Delta = -4.67 \times 10^{-2} \text{ cm}^{-1}$, $zJ' = -0.14 \text{ cm}^{-1}$ for complex **2**. The negative zJ' values are indicative of the antiferromagnetic interactions between paramagnetic species in complexes **1** and **2**^[24-25].

The magnetic interactions and corresponding distances of these complexes are listed in Table 2. By comparison, it can be found that similar complexes have zJ' values within a

certain range. With the bond length of $O_{\text{Rad}}\text{-Tb(III)}$ decrease, the magnetic interaction turn to strong, thus, the value of zJ' increase. However, Dy complexes do not play this rule, this maybe due to the fitting model ignoring some magnetic effect.

Table 2. The magnetic interactions and corresponding distances reported of complexes **1-2** in the literatures.

| Complexes | $O_{\text{Rad}}\text{-Tb(III)}$ (Å) | $\Delta(\text{cm}^{-1})$ | $zJ'(\text{cm}^{-1})$ | ref |
|--|-------------------------------------|--------------------------|-----------------------|-----------|
| [Tb(hfac) ₃ (NITPh-3-Br-4-OMe) ₂] | 2.355 | -0.190 | -0.090 | 18 |
| [Tb(hfac) ₃ (NITPh-Pa) ₂] ^[a] | 2.333 and 2.335 | -0.120 | -0.070 | 19 |
| Tb(hfac) ₃ (NITPh-(OCH ₃) ₂) ₂ | 2.331 | -0.565 | -0.145 | this work |
| Complexes | $O_{\text{Rad}}\text{-Dy(III)}$ (Å) | $\Delta(\text{cm}^{-1})$ | $zJ'(\text{cm}^{-1})$ | ref |
| [Dy(hfac) ₃ (NITPh-3-Br-4-OMe) ₂] | 2.362 | -0.050 | +0.070 | 18 |
| Dy(hfac) ₃ (NITPhSCF ₃) ₂ ^[b] | 2.310 and 2.329 | -0.0101 | -0.0538 | 19 |
| [Dy(hfac) ₃ (NITPh-Pa) ₂] | 2.316 and 2.322 | -0.070 | -0.080 | 20 |
| {Dy(hfac) ₃ [NITPhp-OCH ₂ CH=CH ₂] ₂ } ^[c] | 2.303 and 2.345 | -0.0005 | -0.0133 | 21 |
| Dy(hfac) ₃ (NITPh-(OCH ₃) ₂) ₂ | 2.325 | -0.0468 | -0.140 | this work |

[a] NITPh-Pa=2-(3',4'-dioxylmethylene-phenyl)-4,4,5,5-tetramethyl-imidazoline-1-oxyl-3-oxide;

[b] NITPhSCF₃ = 2-(4-trifluoromethylthiophenyl)-4,4,5,5-tetramethylimidazoline-1-oxyl-3-oxide;

[c] NITPhp-OCH₂CH=CH₂=2-(4'-Alloxyphenyl)-4,4,5,5-tetramethylimidazoline-1-oxyl-3-oxide.

The results of alternating current susceptibility of complexes **1** and **2** show that there are no non-zero out-of-phase signal, indicating that there is no slow magnetic relaxation^[26]. Therefore, complexes **1** and **2** have no single molecule magnet behavior. This may be resulted from the fact that a small energy barrier cannot prevent the reversal of spins^[27-28]. The test charts are shown in Figs. S6 and S7, respectively. (test conditions: 0 DC field, 961 Hz, 3.0 Oe AC electric field, temperature: 2-12 K.)

3.4. Luminescence Properties of complex **1**

The luminescent properties of complex **1** were measured at room temperature. Considering that complex **1** has excellent stability in aqueous systems, a series of fluorescence experiments were performed in aqueous solution (Fig. S4). The peak at 312 nm is a $\pi \rightarrow \pi^*$ transition absorption peak caused by the conjugated double bond on the benzene ring, while the absorption peak at 219 nm is attributed to the $\pi \rightarrow \pi^*$ transition absorption band generated by the conjugated group of the ONCNO fragment. The fluorescence spectrum also shows the characteristic emission peak of Tb(III) ions at 336 nm excitation (Fig. S8). The luminescence peaks centered around at 360, 548.5, 94, and 46.5 nm can be belong to the transitions of $^5D_4 \rightarrow ^7F_J$ ($J = 3, 4, 5$ and 6) of complex **1** (Fig. 4). Among these emission peaks, $^5D_4 \rightarrow ^7F_5$ caused by the electron dipole transition has the strongest emission at 548.5 nm^[29-30].

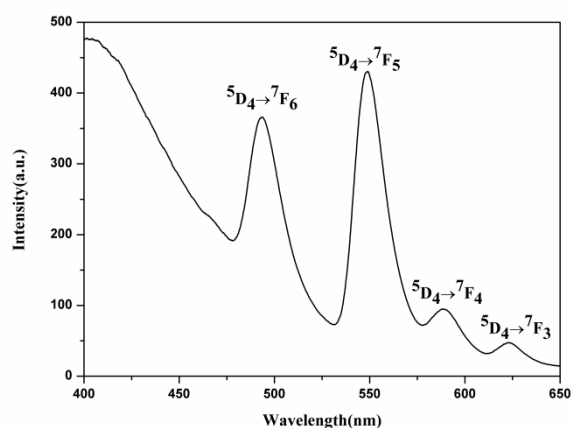


Fig. 4. Emission spectrum in aqueous solution.

Furthermore, in order to study the effect of different anions on the fluorescence intensity of complex **1**, the prepared crystal sample of complex **1** was grinded and dispersed in a salt solutions of K_yX ($X = Cl^-$, SO_4^{2-} , Br^- , NO_3^- , I^- , and $Cr_2O_7^{2-}$), $y = 1$ or 2), and finally a suspension was formed by an ultrasonic method. It is clear that the $Cr_2O_7^{2-}$ anion has a pronounced fluorescence quenching effect on the complex **1**, while other anions have little effect on the fluorescence intensity (Fig. 5). To test the selectivity of complex **1**, interference experiment was performed (Fig. S9). The $Cr_2O_7^{2-}$ anion added to other anionic solution, the fluorescence intensity decreased immediately, then we could observe the quenching of $Cr_2O_7^{2-}$ to achieve the detection of $Cr_2O_7^{2-}$ ^[31-38] in water. With the increases of $Cr_2O_7^{2-}$ concentration, the intensity of luminescence gradually decreases (Fig. 6). In addition, the quenching effect can be analyzed by the Stern-Volmer equation: $I_0/I = 1 + K_{sv}[A]$, in which K_{sv} is quenching constant (M^{-1}), I_0 and I are the fluorescence intensities of complex **1** before and after the addition of anions, $[A]$ is the molar concentration of anions (mM), respectively^[39].

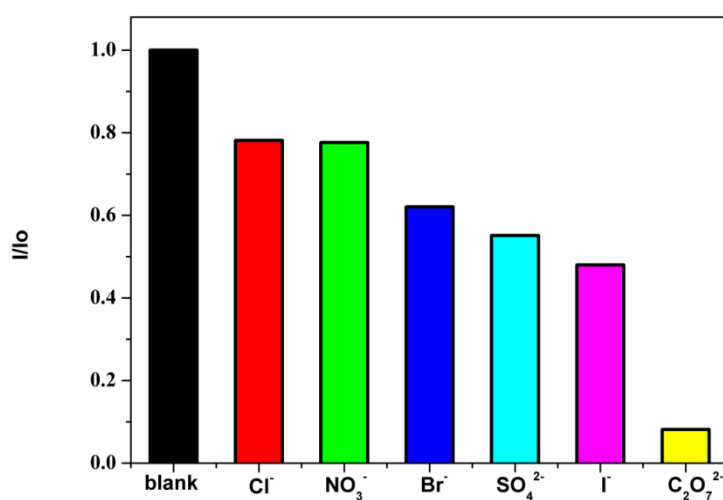


Fig. 5. Luminescence intensity of the transition (548.5nm) of complex **1** in different anions salt solution (1mM). I and I_0 denote the fluorescence intensity of complex **1** in anions solution and water, respectively.

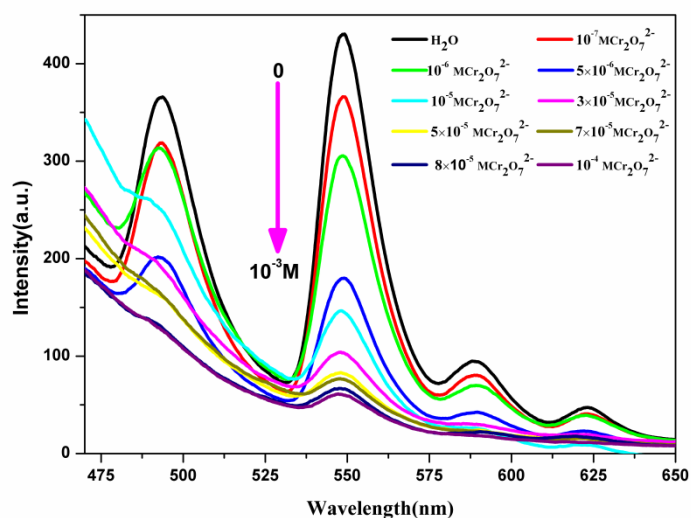


Fig. 6. Emission spectra of complex **1** with different concentration of $\text{Cr}_2\text{O}_7^{2-}$ aqueous solution (from 0 to 10^{-3} M).

The Stern-Volmer quenching curve for $\text{Cr}_2\text{O}_7^{2-}$ anion display linear at low concentrations (from 10^{-7} to 10^{-4} M) (Fig. 7), with a correlation coefficient of 0.982, however the Stern-Volmer quenching curve off-linear at high concentrations. This phenomenon illustrates the quenching of static and dynamic processes. The value of K_{sv} is approximated as $2.10 \times 10^4 \text{ M}^{-1}$. According a ratio of $3\delta/k$, further detailed analysis showed that the detection limit was 10^{-7} M of $\text{Cr}_2\text{O}_7^{2-}$ anion^[40]. Compared with the MOFs listed in Table S6, the detection limit is very low, which means that it is very promising in the selective and sensitive test for $\text{Cr}_2\text{O}_7^{2-}$.

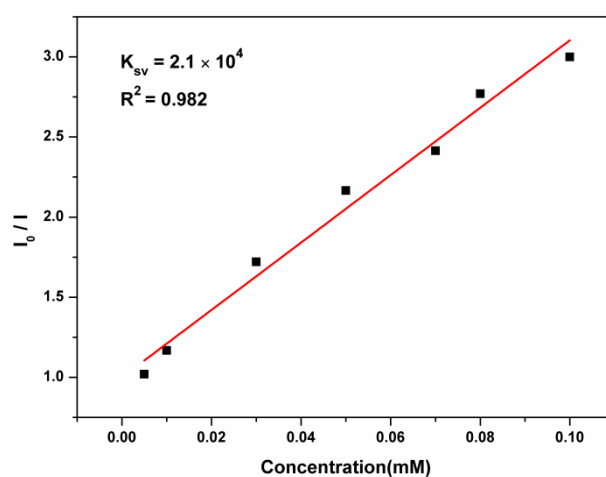


Fig. 7. The Stern-Volmer plot of I_0/I versus the concentration of $\text{Cr}_2\text{O}_7^{2-}$ for complex **1** at low concentration (from 10^{-7} to 10^{-4} M).

In order to further analyze the possible quenching mechanism of $\text{Cr}_2\text{O}_7^{2-}$ anion^[41]. The UV excitation spectrum of the Tb complex overlap strongly with the absorption spectrum of the $\text{Cr}_2\text{O}_7^{2-}$ anion, while other anions have almost no overlap with this wavelength range (Fig. S10). Therefore, the aqueous solution containing $\text{Cr}_2\text{O}_7^{2-}$ anion can forcefully absorb the energy of the excitation wavelength, reducing the energy transfer efficiency from the nitronyl nitroxide radical to the Tb(III) ion, eventually leading to the quenching of luminescence^[42].

4. Conclusions

To sum up, we successfully obtained two mononuclear tri-spin crystals ($[\text{Ln}(\text{hfac})_3(\text{NITPh}-(\text{OCH}_3)_2)_2]$ (Ln(III)=Tb(**1**), Dy(**2**)) by using 3,4-dimethoxyphenyl nitronyl nitroxide radical. The variable temperature magnetic susceptibility of complexes **1** and **2** indicates that there are antiferromagnetic interactions between the Ln(III) ions and radicals in complexes **1** and **2**. Ac magnetic studies of complexes **1** and **2** did not show frequency dependence, indicating that these two complexes may not exhibit SMM behavior. Besides, the fluorescence spectrum of the complex **1** showed the characteristic emission peak of the Tb(III) ion and had the ability to identify the $\text{Cr}_2\text{O}_7^{2-}$ anion. Because of the lower detection limit (1×10^{-7} M) and almost linear at low concentration, complex **1** may potentially sensitive detection of $\text{Cr}_2\text{O}_7^{2-}$ anion and serve as a luminescence-based sensor for quantitative analysis.

Acknowledgements

This work was supported by the National Natural Science Foundation of China (Nos. 21371104, 20771081, 21101096, and 21471084) and Laboratory Innovation Fund (30003) of Tianjin University of Science and Technology.

Appendix A. Supplementary data

CCDC 1830531(1), 1830532(2) contain the supplementary crystallographic data for this paper. These data can be obtained free of charge from The Cambridge Crystallographic Data Centre via www.ccdc.ac.uk/data_request/cif.

References

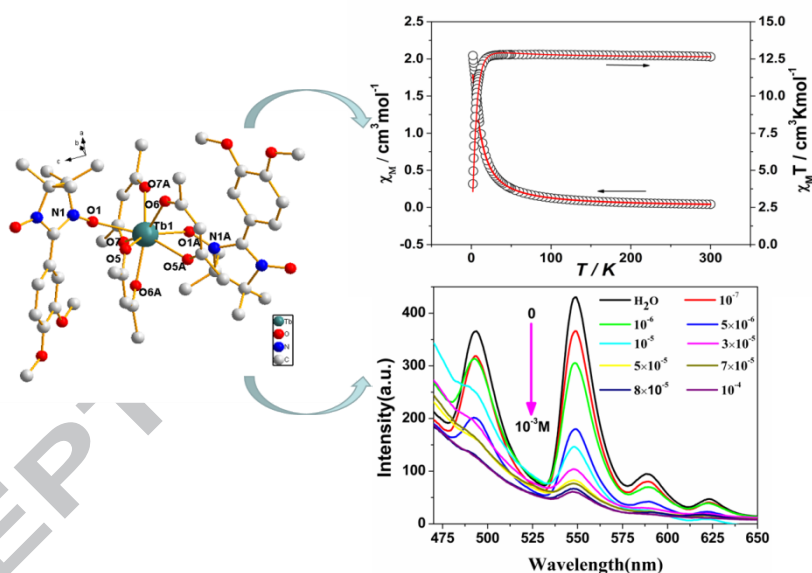
- [1] D. Bhattacharya, S. Shil, T. Goswami, A. Misra, A. Panda, D.J. Klein. *Comput. Theor. Chem.* 1024 (2013) 15.
- [2] S.Y. Zhou, T. Li, X. Li, Y.Q. Sun, Q.L. Wang, D.Z. Liao, L. Tian. *Inorg. Chem. Acta.* 444 (2016) 131.
- [3] F. Mathever, D. Luneau, *J. Am. Chem. Soc.* 123 (2001) 7465.
- [4] R.N. Liu, L.C. Li, X.Y. Xing, D.Z. Liao, *Inorg. Chim. Acta.* 362 (2009) 2253.
- [5] E. Lucaccini, J.-J. Baldoví, L. Chelazzi, A.-L. Barra, F. Grepioni, J.-P. Costes, L. Sorac, *Inorg. Chem.* 56 (2017) 4728.
- [6] N. Zhou, Y. Ma, C. Wang, G.F. Xu, J.K. Tang, S.P. Yan, D.Z. Liao, *J. Solid. State Chem.* 183 (2010) 927.
- [7] A.M. Ako, V. Mereacre, R. Clérac, I.J. Hewitt, Y. Lan, G. Buth, C.E. Anson, A.K. Powell, *Inorg. Chem.* 48 (2009) 6713.
- [8] S.K. Langley, B. Moubaraki, C.M. Forsyth, I.A. Gass, K.S. Murray, *Dalton Trans.* 39 (2010) 1705.
- [9] G. Poneti, K. Bernot, L. Bogani, A. Caneschi, R. Sessoli, W. Wernsdorfer, D. Gatteschi, *Chem. Commun.* 0 (2007) 1807.

- [10] J. Rocha, C.D.S. Brites, L.D. Carlos, *Chem-Eur. J.* 22 (2016) 14782.
- [11] B. Liu, W.P. Wu, L. Hou, Y.Y. Wang, *Chem. Commun.* 50 (2014) 8731 .
- [12] A. G. Brook, D. G. Anderson, J. M. Duff, P. F. Jones, D. M. MacRae, *J. Am. Chem. Soc.* 90 (1968) 1078.
- [13] E. F. Ullman, J. H. Osiecki, D. G. B. Boocock, R. Darcy, *J. Am. Chem. Soc.* 94 (1972) 7049.
- [14] G. A. Bain, J. F. Berry, *J. Chem. Educ.* 85 (2008) 532.
- [15] T. Shiga, M. Ohba, H. Okawa, *Inorg. Chem. Commun.* 6 (2003) 15.
- [16] O.V. Dolomanov, L.J. Bourhis, R.J. Gildea, J.A.K. Howard, H.J. Pushmann, *Appl. Crystallogr.* 42 (2009) 339.
- [17] J.de O. Cabral, M.F.Cabral, M.G.B. Drew, S.M. Nelson, A. Rodgers, *Coord. Chem. Rev.* 24 (1977) 177.
- [18] Y.L. Wang, Y.Y. Gao, Y. Ma, Q.L. Wang, L.C. Li, D.Z. Liao, *J. Solid. State Chem.* 202 (2013) 276.
- [19] M.Y. Song, Y.F. Hou, L.M. Wen, S.P. Wang, S.T. Yang, J.J. Zhang, L.N. Geng, S.K. Shi, *J. Mol. Struct.* 1107 (2016) 174.
- [20] S.L. Yang, R.R. Wang, X.J. Jin, C.X. Zhang, Q.L. Wang, *Polyhedron.* 144 (2018) 101.
- [21] C.X. Zhang, H.W. Chen, W.M. Wang, Y.Y. Zhang, *Inorg. Chem. Commun.* 24 (2012) 177.
- [22] M.C. Majee, S. M. T. Abtab, D. Mondal, M. Maity, M. Weselski, M. Witwicki, A. Bienko, M. Antkowiak, G. Kamieniarz, M. Chaudhury, *Dalton trans. (Cambridge, England).* 47 (2003) 3425.
- [23] M. K. Singh, T. Rajeshkumar, R. Kumar, S. K. Singh, G. Rajaraman. *Inorg. Chem.* 57 (2018) 1846.
- [24] S. Chorazy, M. Rams, M. Wyczesany, K. Nakabayashi, S.-i. Ohkoshi, B. Sieklucka, *CrystEngComm.* 20 (2018) 1271.
- [25] M. L. Kahn, J. P. Sutter, S. Golhen, P. Guionneau, L. Ouahab, O. Kahn, D. Chasseau, *J. Am. Chem. Soc.* 122 (2000) 3413.
- [26] P. Albores, J. Seeman, E. Rentschler, *Dalton trans.* 37 (2009) 7660.
- [27] T. Kajiwara, K. Takahashi, T. Hiraizumi, S. Takaishi, M. Yamashita, *CrystEngComm.* 11 (2009) 2110;
- [28] T. Kajiwara, M. Nakano, K. Takahashi, S. Takaishi, M. Yamashita, *Chem-Eur. J.* 17 (2011) 196.
- [29] S. Swavey, R. Swavey, *Coord. Chem. Rev.* 253 (2009) 2627.
- [30] Z. Ahmed, K. Iftikhar, *Inorg. Chem. Acta.* 392 (2012) 165.
- [31] Z. Sun, M. Yang, Y. Ma, L.C. Li, *Cryst. Growth Des.* 17 (2017) 4326.
- [32] G.X. Wen, M.L. Han, X.Q. Wua, Y.P. Wua, W.W. Donga, J. Zhaoa, D.S. Li, L.F. Ma, *Dalton Trans.* 45 (2016) 15492.
- [33] G.P. Li, G. Liu, Y.Z. Li, L. Hou, Y.Y. Wang, Z.H. Zhu, *Inorg. Chem.* 55 (2016) 3952.
- [34] C.H. Zhang, L.B. Sun, Y. Yan, H.Z. Shi, *J. Mater. Chem. C.* 5 (2017) 8999.
- [35] R.C. Gao, F.S. Guo, N.N. Bai, Y.L. Wu, F. Yang, J.Y. Liang, Z.J. Li, Y.Y. Wang, *Inorg. Chem.* 55 (2016) 11323.
- [36] X.Y. Xu, B. Yan. *ACS Appl. Mater. Interfaces.* 7 (2015) 721.
- [37] J.J. Liu, G.F. Ji, J.N. Xiao, Z.L. Liu, *Inorg. Chem.* 56 (2017) 4197.

- [38] T.Y. Gu, M. Dai, D. J. Young, Z.G. Ren, J.P. Lang, *Inorg. Chem.* 56 (2017) 4668.
 [39] A. Martin-Barreiro, S. de Marcos, J. Galban, *Microchem. Acta.* 185 (2018) 171.
 [40] X.L. Zhao, D. Tian, Q. Gao, H.W. Sun, J. Xu, X.H. Bu, *Dalton Trans.* 45 (2016) 1040;
 [41] J.M. Zhou, W. Shi, H.M. Li, H. Li, P. Cheng, *J. Phys. Chem. C.* 118 (2014) 416.
 [42] M. Eltermann, V. Kiisk, A. Berholts, L. Dolgov, S. Lange, K. Utt, R. Jaaniso, *Sensor. Actuat. B-Chem.* 265 (2018) 556.

Graphical Abstract

In complexes **1** and **2**, isolated mononuclear molecules connect each other through intermolecular hydrogen bonds to form 3D supermolecular framework. Quantitative estimate of the magnetic interaction parameters between paramagnetic species in complexes **1** and **2**, The result indicates that there are weak antiferromagnetic interaction between metal ions and nitronyl nitroxide radicals. The study of luminescence properties show that complex **1** may potentially detect $\text{Cr}_2\text{O}_7^{2-}$ anions sensitively and as a luminescence-based sensor for quantitative analysis, due to the lower detection limit (1×10^{-7} M) and almost linear at low concentrations.



Graphical abstract synopsis

1. In complexes **1** and **2**, isolated mononuclear molecules connect each other through intermolecular hydrogen bonds to form 3D supermolecular framework.
2. Quantitative estimate of the magnetic interaction parameters between paramagnetic species in complexes **1** and **2**, The result indicates that there are weak antiferromagnetic interaction between metal ions and nitronyl nitroxide radicals
3. The study of luminescence properties show that complex **1** may potentially detect $\text{Cr}_2\text{O}_7^{2-}$ anions sensitively and as a luminescence-based sensor for quantitative analysis, due to the lower detection limit (1×10^{-7} M) and almost linear at low concentrations.